International Journal of Automotive Technology, Vol. ?, No. ?, pp. ?−?(year)

Serial#Given by KSAE

ONLINE DETECTION OF TOE ANGLE MISALIGNMENT BASED ON LATERAL TIRE FORCE AND TIRE ALIGNING MOMENT

Hwangjae Lee and Seibum B. Choi*

Department of Mechanical Engineering, KAIST, Daejeon 34141, Korea

(*Received date ; Revised date ; Accepted date*)

ABSTRACT− Wheel alignment of a vehicle composed of toe, camber and caster is essential for stable driving. Among them, the toe angle can be easily adjusted in many commercial vehicles when misaligned. However, there have been many difficulties for a driver to directly detect the misalignment of the toe angle. To solve this problem, this paper proposes a novel system that detects misaligned toe angle in real-time by utilizing the lateral tire force and tire aligning moment. The system is largely divided into the lateral tire force model construction, tire aligning moment model construction, and misalignment detection. During the lateral tire force model and the tire aligning moment model construction, linearized recursive least squares are used to identify parameters necessary for the building of the models. Afterwards, during the misalignment detection, the misaligned toe angle is detected in real-time without additional sensors by estimating the slip angle of each wheel reflecting the toe angle effect based on these two models. The proposed system is verified by the vehicle dynamics software CarSim, and the simulation results show that misaligned toe angle can be successfully detected in real-time while driving.

KEY WORDS : Wheel alignment, Recursive least squares, Parameter adaptation, Camber, Toe, Slip angle

NOMENCLATURE

F_z	: tire normal force
l_f	: center of gravity-front axle distance
l_r	: center of gravity-rear axle distance
v_x	: longitudinal speed
v_y	: lateral speed
k	: discretized time step
y	: measurement (system output)
v	: measurement noise
a_{cpl0}	: half of tire contact patch length at idle
F_{z0}	: tire normal force at idle

1. INTRODUCTION

A vehicle needs proper wheel alignment settings throughout its life cycle, which plays an important role in improving driving performance and stability (Dechao, W. and Yaqing, T., 2007; Mananathan, R., 2021). One of the most important and easily adjustable factors in wheel alignment settings is the toe angle (Furferi *et al.*, 2013). As shown in Figure 1, the toe angle refers to the symmetrical angle between the tires and the longitudinal axis of the vehicle when the vehicle is viewed from above (Spike *et al.*, 2019). If the leading edges of the two front wheels of the vehicle are slightly facing each other, it is called "toe-in", and if the leading edges of the two wheels are in a position to move away from each other, it is called "toe-out". The setting of the toe angle affects tire wear, straight driving and corner entry handling characteristics (Furferi *et al.*, 2013). In other words, if the toe angles are not symmetrical with each other or misaligned, it can affect not only partial tire wear, but also steering and overall stability of the vehicle (Patel, 2016).

However, the problem is that it is not easy for a driver to detect such misalignment. Usually, the driver sees the condition of irregularly worn tires and suspects the misalignment. In the end, the driver receives a detailed wheel alignment inspection. In this case, since tire wear due to misalignment has already progressed, replacement of worn tires as well as wheel alignment is required for safe driving.

Since it is important to preemptively detect wheel misalignment, studies have been conducted to detect it before any signs of misalignment appear (D'Mello *et al.*, 2022; Sulaiman *et al.*, 2021; Gajek and Strzępek, 2016).

* *Corresponding author*. e-mail: sbchoi@kaist.ac.kr

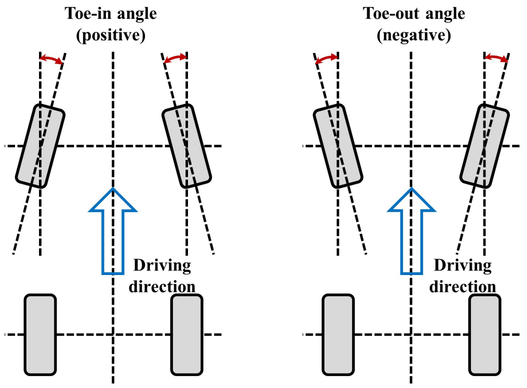

Figure 1. Wheel alignment (Toe).

D'Mello *et al.* (2022) proposed a user-friendly and low-cost wheel alignment system using PU6050 sensor and ESP32 microcontroller. Gajek and Strzępek (2016) introduced a smaller and portable wheel alignment monitoring system using sensors and mobile phone application. Lastly, Sulaiman *et al.* (2021) presented the examination of the wheel alignment inspection method on the slide slip plate stand which is an obligatory test during a periodic technical inspection of the vehicle. The studies mentioned above focused more on precise measurement of wheel alignment components than wheel misalignment detection itself. Thus, toe and camber angles can be measured to a certain level, but the use of additional equipment and sensors such as microcontrollers, gyro sensors, and accelerometers is inevitable. Also, since most of them focus more on detailed angle measurement, those are not effective in real-time detection of misalignment while driving.

Detecting wheel misalignment during driving without additional sensors has been left as a challenging problem. One reason is that toe and camber angles have a complex relationship with vehicle body and suspension dynamics (Henning and Sawodny, 2016). However, in the case of toe angle, one can focus on the fact that the information of the toe angle can be directly reflected and expressed in the slip angle of each wheel. Taking this advantage, it is realizable to determine the misalignment of the toe angle based on the information of asymmetric slip angles.

In this paper, the authors propose a novel system for real-time detection of misaligned toe angles in a driving condition by utilizing the lateral force and alignment moment of the tire on the basis of the above-mentioned concept. The system first identifies the parameters necessary for constructing the lateral tire force model and tire aligning moment model using linearized recursive least squares (LRLS). This is because the toe angle affects the slip angle of each wheel and the lateral force and aligning moment of the tire can be expressed as a function of the slip angle. Once the parameters of the two

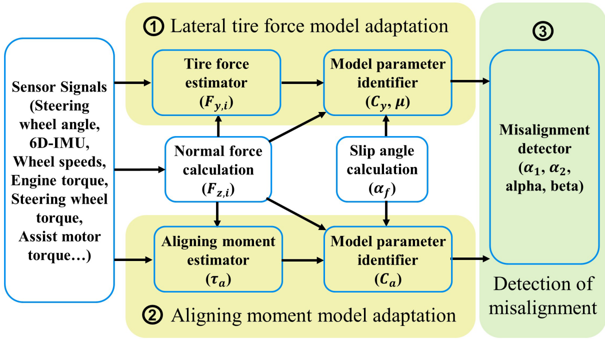

Figure 2. Flow structure of the system.

models are identified, it is possible to determine whether the toe angle is misaligned by estimating and comparing the slip angle of each wheel that has the information of toe angle based on the constructed models. What sets this system apart from previous studies is that it can detect misalignment of the toe angle in real-time while driving only with sensor signals available from a commercial vehicle.

This paper is constructed as follows. The overall system architecture is described in Section 2. Lateral tire force model adaptation is covered in section 3. Tire aligning moment model adaptation is described in Section 4, and the design of misalignment detector is dealt with in Section 5. In Section 6, we analyze the proposed system through CarSim/Simulink co-simulation platform and conclude the paper in Section 7.

2. STRUCTURE OF THE SYSTEM

The system is composed of three parts as shown in Figure 2: adaptation of the lateral tire force model, adaptation of the tire aligning moment model, and the determination of misalignment. First, in the lateral tire force model adaptation step, the brush tire model is fitted to the lateral tire force estimated from vehicle dynamics. In this process, parameters in the model such as tire coefficient of lateral force C_y and tire-road friction coefficient μ are adapted. As for the tire-road friction coefficient, it is also used in the next step.

The second step proceeds in a similar manner to the first step by fitting the tire aligning moment model to the tire aligning moment that can be estimated in a vehicle equipped with electric power steering (EPS). One parameter to be adapted in this process is the tire coefficient of aligning moment C_a. Once this step is completed, preparations for estimating the slip angle of each wheel reflecting the effect of the toe angle are completed.

The third and final step is the toe angle misalignment detection. In this step, an unknown offset is given to the left and right wheels based on the slip angle of the front axle estimated from the vehicle dynamics, and then this offset value is estimated using the two previously adapted models. Since this value includes the effect of toe angle, which is difficult to calculate with vehicle kinematics and dynamics, it is possible to detect toe angle misalignment by comparing these offset values.

3. LATERAL TIRE FORCE MODEL ADAPTATION

3.1. Model Selection and Tire Force Estimation

In order to fit the tire model according to the estimated lateral tire force, it is important to select an appropriate tire model. Since this study focuses on prompt parameter identification for real-time implementation, a model with a small number of parameters is suitable. Among many tire models, the brush tire model (Pacejka, 2005) satisfies this requirement because it contains only stiffness and friction parameters while expressing the nonlinearity of the tire precisely (Choi and Choi, 2014).

To further increase the accuracy of parameter identification, this system considers only the pure lateral slip case excluding longitudinal tire slip. The toe angle misalignment detection system has no problem in its performance even when it uses data acquired under ideal driving conditions over a relatively long period of time. Therefore, the accuracy of the model can be further improved by focusing on the situation where the vehicle has pure lateral slip without braking or acceleration.

In a pure lateral slip case, the lateral tire force can be expressed as follows:

$$F_y = \begin{cases} -C_y \tan(\alpha) + \left(\dfrac{1}{3}\dfrac{C_y^2 \left|\tan(\alpha)\right| \tan(\alpha)}{\mu F_z}\right) \\ -\left(\dfrac{1}{27}\dfrac{C_y^3 \tan^3(\alpha)}{(\mu F_z)^2}\right) & \text{for } |\alpha| \le \left|\alpha_{sl\_force}\right| \\ -\mu F_z \operatorname{sgn}(\alpha) & \text{for } |\alpha| \ge \left|\alpha_{sl\_force}\right| \end{cases} \tag{1}$$

where F_y, α, and α_{sl_force} stand for the lateral tire force, slip angle, and slip angle at which the tire has lost lateral grip. α_{sl_force} can also be expressed as follows:

$$\alpha_{sl\_force} = \tan^{-1}\left(\frac{3}{C_y I_f}\right), \quad I_f = \frac{1}{\mu F_z} \tag{2}$$

Here, I_f denotes the inverted peak friction limit.

To utilize the selected model for lateral tire force model adaptation, the lateral tire force estimation must be preceded. Studies on lateral tire force estimation have been conducted in a wide variety of cases, and the estimation results are often satisfactory (Rezaeian *et al.*, 2014; Xu *et al.*, 2022; Lee *et al.*, 2018). In this system,

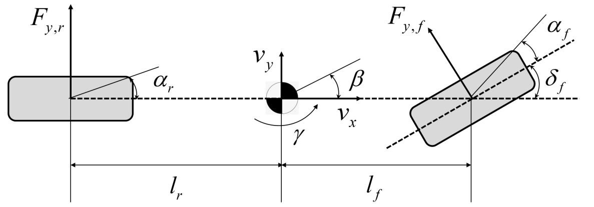

Figure 3. Bicycle model for front and rear axle slip angle estimation.

the front lateral axle force $F_{y,f}$ and rear lateral axle force $F_{y,r}$ are estimated by the tire force estimation method in Cho *et al.* (2009) using the random walk Kalman filter. The vertical force acting on each wheel $F_{z,i}$ can also be estimated without difficulty (Doumiati *et al.*, 2009). Additionally, by using the vertical force distribution of the left and right wheels of each axis, the lateral force acting on each wheel $F_{y,i}$ can be obtained (Rezaeian *et al.*, 2014). Here, i = 1, 2, 3, 4, which correspond to the left-front, right-front, left-rear, and right-rear wheels, respectively.

In addition to the tire force, the slip angle of each wheel α_i matched to each tire force are also utilized for lateral tire force model adaptation. At this point, it is possible to obtain and apply the slip angles of the front and rear axles which can be estimated relatively easily from the vehicle model shown in Figure 3 (Rajamani, 2011; Gadola *et al.*, 2014; Lee and Choi, 2022). This is expressed as:

$$\begin{aligned} \alpha_f &= \beta + \frac{l_f \gamma}{v_x} - \delta_f \\ \alpha_r &= \beta - \frac{l_r \gamma}{v_x} \end{aligned} \tag{3}$$

where α_f, α_r, β, γ, and δ_f denote the tire slip angle of front and rear axles, side-slip angle, yaw rate, and front steering angle respectively.

3.2. Model Adaptation using LRLS

The parameters that requires adaptation in the lateral tire force model are C_y and μ, and are identified through the recursive least squares method. The least square method is a method of fitting a mathematical model to a set of data by minimizing the sum of the squares of the difference between the observed data and the data obtained from the model. However, the general least squares method has the disadvantage of having to recalculate all data including new data when the new one has been acquired. Compensating for this drawback is the recursive least squares method, which can be expressed as (Teunissen, 2001):

$$\hat{\theta}(k) = \hat{\theta}(k-1) + K(k)\left(y(k) - \phi^T(k)\hat{\theta}(k-1)\right) \quad (4)$$

where

$$y(k) = \phi^T(k)\theta + v$$
$$K(k) = \frac{P(k-1)\phi(k)}{\lambda + P(k-1)\phi^2(k)}$$
$$P(k) = \frac{1}{\lambda}\left[P(k-1) - \frac{P^2(k-1)\phi^2(k)}{\lambda + P(k-1)\phi^2(k)}\right]$$

Here, θ, K, P, and λ are the unknown parameter, update gain, error covariance and forgetting factor respectively.

Additionally, since this algorithm is only suitable for linear systems, it is necessary to transform the equation to apply it to the brush model with non-linearities. For this, $y(k)$ can be approximated as follows considering it is a nonlinear form (Choi *et al.*, 2013):

$$\begin{aligned} y(k) &= f(k,\theta) + v \\ y(k) &\approx F(k)\left(\hat{\theta}(k) - \hat{\theta}(k-1)\right) + f\left(\hat{\theta}(k-1), k\right) \end{aligned} \quad (5)$$

where

$$F(k) = \left.\frac{\partial f(\theta,k)}{\partial \theta}\right|_{\theta=\hat{\theta}(k-1)}$$

Then, an arbitrary function $z(k)$ consisting of measurable and computable terms is defined as follows:

$$z(k) = y(k) + F(k)\left(\hat{\theta}(k-1)\right) - f\left(\hat{\theta}(k-1), k\right) \quad (6)$$

Substituting $y(k)$ approximated in Equation (5) into Equation (6) gives the following linearized expression:

$$z(k) \approx F(k)\hat{\theta}(k) \quad (7)$$

Since Equation (7) has the same format as $y(k)$ in Equation (4), a state update expression reflecting the nonlinearity of the brush tire model can be derived as follows by replacing $\phi^T(k)$ with $F(k)$ and $y(k)$ with $z(k)$:

$$\hat{\theta}(k) = \hat{\theta}(k-1) + K(k)\left(z(k) - F(k)\hat{\theta}(k-1)\right) \quad (8)$$

where

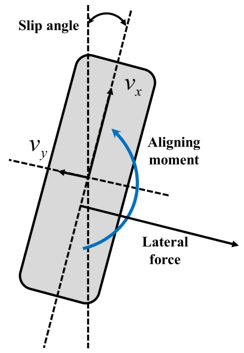

Figure 4. Tire aligning moment.

$$\theta(k) = \left[C_y \ \mu\right]^T$$

θ, a parameter to be adapted, is updated whenever $F_{y,i}$ is newly acquired. As mentioned above, a lateral tire force model very similar to the actual behavior can be constructed by taking the advantage that the fitting can be performed in a driving environment suitable for model adaptation

4. TIRE ALIGNING MOMENT MODEL ADAPTATION

4.1. Model Selection and Tire Aligning Moment Estimation

As shown in Figure 4, the tire aligning moment is the moment to return the tire to its original position, also called self-aligning torque. Basically, the tire aligning movement is generated about the steer axis by lateral tire force. The aligning moment can be expressed as a function of the tire slip angle, like the lateral tire force, and can be estimated in a vehicle equipped with EPS (Yasui *et al.*, 2004; Hsu *et al.*, 2009). In this paper, it is assumed that the value of the aligning moment can be readily available based on the previous research (Ma *et al.*, 2018). The tire steering torque is first obtained as a disturbance observer and utilized to obtain the aligning moment. Ma *et al.* (2018) can be referred to for details. The slip angle of the front axle acquired from Equation (3) is also utilized for the adaptation.

The aligning moment model used in this study uses the same brush model as the previous tire model. The aligning moment based on the brush model is expressed as:

$$\tau_a = \begin{cases} \dfrac{C_a \tan(\alpha) a_{cpl}}{3}\left(1 - \left|\dfrac{C_a \tan(\alpha)}{3\mu F_z}\right|\right)^3 & \text{for } |\alpha| \le |\alpha_{sl\_moment}| \\ 0 & \text{for } |\alpha| \ge |\alpha_{sl\_moment}| \end{cases}$$

(9)

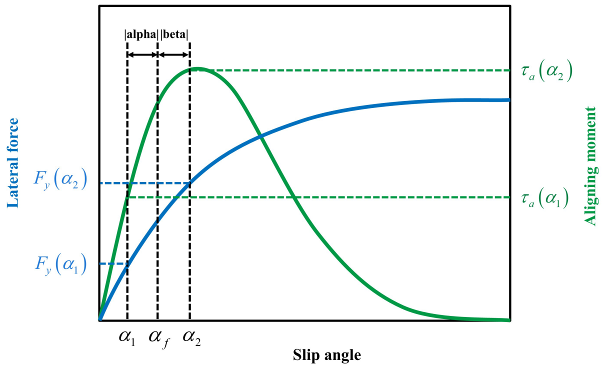

Figure 5. Lateral tire force and tire aligning moment curves.

where

$$a_{cpl} = a_{cpl0}\sqrt{\frac{F_z}{F_{z0}}},\quad \alpha_{sl\_moment} = \tan^{-1}\left(\frac{3}{C_a I_f}\right)$$

Here, τ_a, α_{cpl}, and α_{sl_moment} represent the tire aligning moment, half the tire-road contact length, and slip angle when the tire starts complete sliding respectively.

To mention one thing, the lateral tire force and the tire aligning moment in the brush model share the same lateral stiffness. However, using their respective coefficients as in Ma *et al.* (2018) better describes the force and moment of the real tire. In accordance with this, C_y and C_a are applied to the lateral tire force and tire alignment moment respectively in this study.

4.2. Model Adaptation using LRLS

Based on the estimated tire aligning moment, one required parameter for adaptation in the aligning moment model is C_a as shown in the following equation:

$$\theta(k) = [C_a] \quad (10)$$

The parameter is identified through the LRLS in the same way as described in Section 3.

5. DESIGN OF MISALIGNMENT DETECTOR

Toe angle misalignment is basically detected by estimating and comparing the slip angle of each front tire which reflects the effect of the toe angle. However, estimating the slip angle of each wheel that reflects the effect of toe angle based on the vehicle kinematics and dynamics is a very complex and challenging problem, and in many cases, it is inevitable to attach additional sensors to obtain the required data for estimation (Erdogan *et al.*, 2010). To overcome these difficulties, a method that simultaneously utilizes the lateral tire force and the tire aligning moment is proposed in this study. This method estimates the slip angle of each wheel reflecting the effect of the toe angle in a relatively simple way.

As shown in Figure 5, the lateral tire force and tire aligning moment can be expressed as a function of the tire slip angle. Here, it is important to express the above two functions for the toe angle misalignment detection. To this end, each model has been adapted in Sections 3 and 4, and the graph shown in Figure 5 can be obtained based on it. In addition to the lateral tire force and tire aligning moment curves, the front lateral axle force $F_{y,f}$, and the front axle aligning moment $\tau_{a,f}$ can also be obtained and are readily available (Rezaeian *et al.*, 2014; Hsu *et al.*, 2009). In Section 3, $F_{y,f}$ was used to estimate the lateral tire force of each wheel $F_{y,i}$ utilizing the normal force, but $F_{y,i}$ in Section 3 ignores the effect of the toe angle and cannot be used for toe angle misalignment detection. However, $F_{y,f}$ itself still contains information about the toe angles of both wheels. The limitation is that $F_{y,f}$ alone cannot give the information of how much each of the left and right wheels contribute to the formation of $F_{y,f}$. $\tau_{a,f}$ also reflects the effect of toe angle towards the left and right tires. However, like $F_{y,f}$, it is impossible to determine how much each of the left and right wheels' aligning moment contribute to the formation of $\tau_{a,f}$ only with the estimated $\tau_{a,f}$. Instead, if $F_{y,f}$ and $\tau_{a,f}$ are considered together, it can be estimated how much contribution of each the left and right wheel have in forming $F_{y,f}$ and $\tau_{a,f}$.

In order to estimate their individual contribution, the relationship shown in Figure 5 can be constructed and expressed as a system of equations as follows:

$$\begin{cases} F_{y,f} = F_y(\alpha_1) + F_y(\alpha_2) \\ \tau_{a,f} = \tau_a(\alpha_1) + \tau_a(\alpha_2) \end{cases} \quad (11)$$

where α_1 and α_2 are the left wheel slip angle and the right wheel slip angle, respectively, reflecting the effect of the toe angle.

When expressed as in Equation (11), since the number of unknowns and equations is the same, the unknown values, that is, the left wheel and right wheel slip angles can be specified. Even so, another issue is that it cannot be guaranteed for two unknowns to always have one unique solution complying with the constructed models. To solve this problem, the LRLS mentioned in the previous section is applied.

Unfortunately, the slip angle of each wheel is a value that changes greatly at every step, so it is very challenging to estimate α_1 and α_2 itself as the LRLS. Therefore, a transformation of the equation into a form suitable for the LRLS is required. For this, the slip angle with respect to the front axle in Equation (3) can be utilized. As mentioned above, α_f can be estimated relatively easily, unlike α_1 and α_2. Although α_f itself does not contain individual information about the toe angle of each wheel, it does reflect the vehicle dynamics. Therefore, if α_1 and α_2 are expressed as functions for α_f, the tire slip angle due to the influence of the toe angle excluding the dynamic component can be specified as a separate unknown parameter as follows:

$$\alpha_1 = \alpha_f + alpha, \quad \alpha_2 = \alpha_f - beta$$
$$\theta(k) = [alpha\ beta]^T \tag{12}$$

Since $alpha$ and $beta$ are predominantly affected by the vehicle's toe angle in a low slip condition, it can be expected as static values that do not change significantly unless the original toe angle changes. That is, it can be recognized as an offset with respect to the slip angle of the front axle obtained through Equation (3).

Finally, when Equation (12) is set as the unknown parameter, Equations (1) and (9) are transformed as follows to be applied to the LRLS:

$$F_{y,f} = \left(\begin{array}{l} -C_y \tan(\alpha_f + alpha) \\ + \left(\dfrac{1}{3} \dfrac{C_y^2 \left|\tan(\alpha_f + alpha)\right| \tan(\alpha_f + alpha)}{\mu F_z} \right) \\ - \left(\dfrac{1}{27} \dfrac{C_y^3 \tan^3(\alpha_f + alpha)}{(\mu F_z)^2} \right) \end{array} \right) + \left(\begin{array}{l} -C_y \tan(\alpha_f - beta) \\ + \left(\dfrac{1}{3} \dfrac{C_y^2 \left|\tan(\alpha_f - beta)\right| \tan(\alpha_f - beta)}{\mu F_z} \right) \\ - \left(\dfrac{1}{27} \dfrac{C_y^3 \tan^3(\alpha_f - beta)}{(\mu F_z)^2} \right) \end{array} \right),$$

$$\tau_{a,f} = \left(\frac{C_a \tan(\alpha_f + alpha) a_{cpl}}{3} \left(1 - \left| \frac{C_a \tan(\alpha_f + alpha)}{3\mu F_z} \right| \right)^3 \right) + \left(\frac{C_a \tan(\alpha_f - beta) a_{cpl}}{3} \left(1 - \left| \frac{C_a \tan(\alpha_f - beta)}{3\mu F_z} \right| \right)^3 \right)$$

(13)

In general, as the slip angle increases, the vertical load and jounce on each wheel could increase, which can have a slight effect on the toe and camber angle (Balike et al., 2011). In addition, in the area where the slip angle is small, as shown in Figure 6, the tire lateral force curve and the tire aligning moment curve have the steepest slope, so the effect of static alignment can be maximized. Considering the above reasons, misalignment detection is carried out for the slip angle corresponding to the shaded area of the operation range graph shown in Figure 6. By doing so, the unwanted effect from vertical load and jounce can be minimized while maximizing the effect of static alignment. This range is before the maximum value of the aligning moment curve. The point at which the aligning moment has a maximum value can be determined through the composite tire model parameter θ_y, which is expressed as:

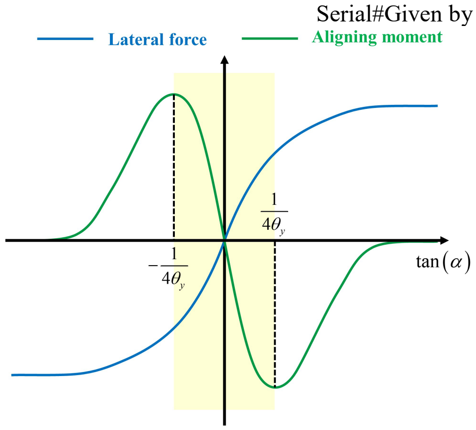

Figure 6. Operation range of the detector.

$$\theta_y = \frac{C_a}{3\mu F_z} \tag{14}$$

θ_y can be obtained explicitly using the parameters estimated during the model adaptations in Sections 3 and 4.

6. SIMULATION ANALYSIS

The performance of the toe angle misalignment detector has been evaluated using the front-wheel driving E-class sedan model in the high-fidelity simulation software, CarSim, in connection with MATLAB/Simulink. The road is assumed to be the most commonly encountered dry road, and is set to have a tire-road friction of 0.9 based on the research in Hahn *et al.*, 2002. The simulation analysis is divided into two sections. The first section discusses model adaptation performance verification, and the second section discusses the results of toe angle misalignment detection.

6.1. Model Adaptation

In order to verify the accuracy of parameter identification during lateral tire model adaptation and tire aligning moment adaptation, a sine wave steering and a constant longitudinal speed are applied as shown in Figure 7(a) and (b). Fig. 7(c) shows the results of identification of parameters C_y and μ, which are estimated in the lateral tire force model. First, μ shows good convergence to the true value of 0.9, and C_y also converges to a constant value. To check whether C_y was correctly estimated along with μ, the actual lateral force value of the left front wheel and the lateral force value calculated from the model to which the estimated parameters were applied are expressed in Figure 7(d). As the two values match each other well, it can be confirmed that not only μ but also C_y are well identified.

Similarly, it can be determined whether C_a, a parameter

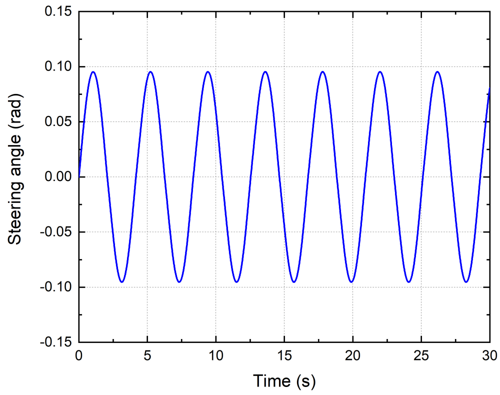

(a) Steering angle

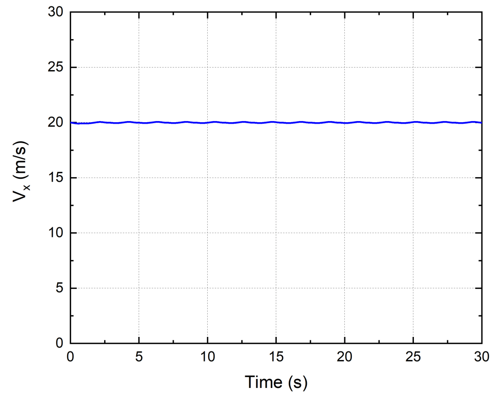

(b) Longitudinal speed

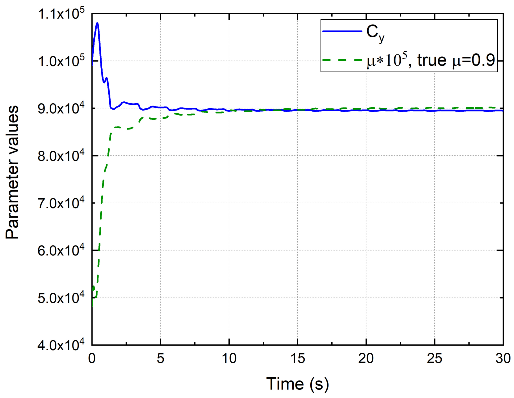

(c) Parameter identification (Lateral force)

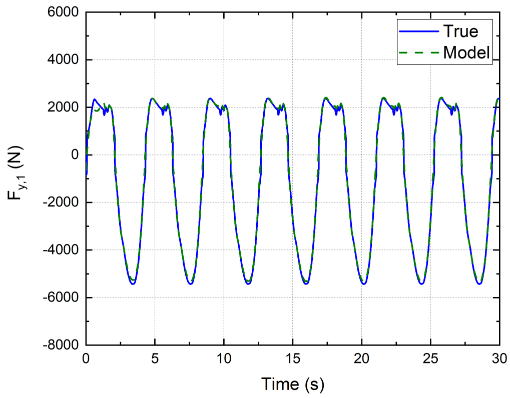

(d) Lateral force

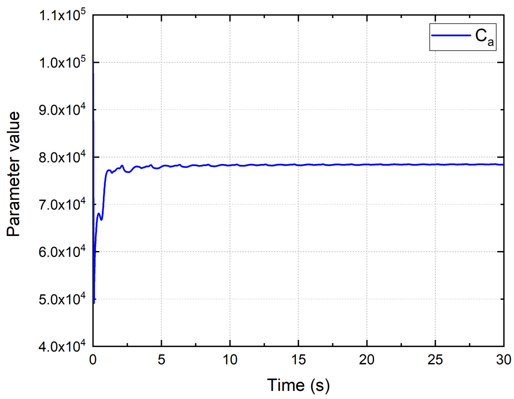

(e) Parameter identification (Aligning moment)

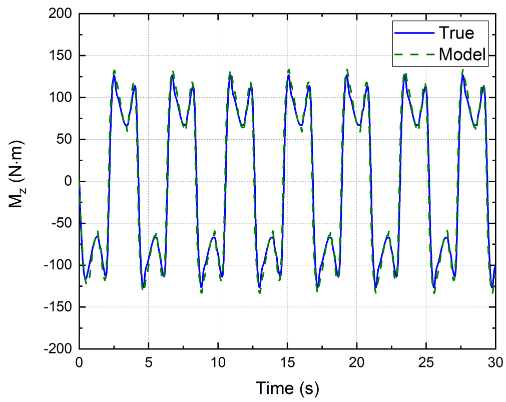

(f) Aligning moment

Figure 7. Simulation results for model adaptation.

Serial#Given by KSAE

estimated in the tire aligning moment model, has been identified properly. Figure 7(e) shows that C_a converges to a constant value over time during the model adaptation. To verify the performance of the adapted model, the curve of the aligning moment value obtained from the model using the estimated parameter values and the curve of the true aligning moment value have been plotted together in Figure 7(f). It can be confirmed that C_a is also well identified as the two values are almost identical.

6.2. Detection of Toe Angle Misalignment

Toe angle misalignment is detected when the slip angle is small as mentioned in Section 5. Considering this, a sine wave steering and a constant longitudinal speed as shown in Figure 8(a) and (b) have been applied to describe the continuous detection situation. Along with

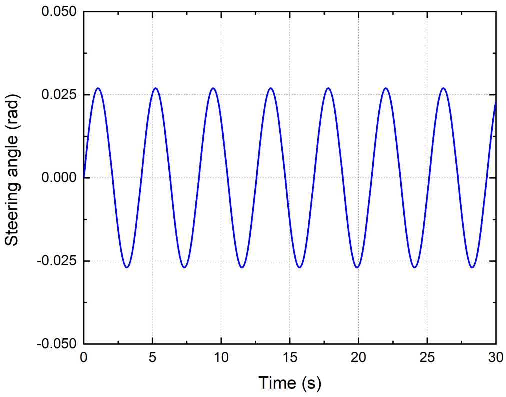

(a) Steering angle

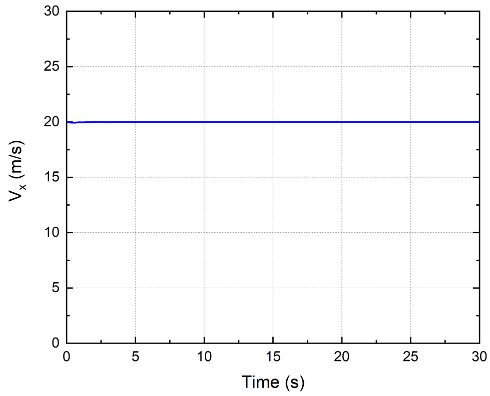

(b) Longitudinal speed

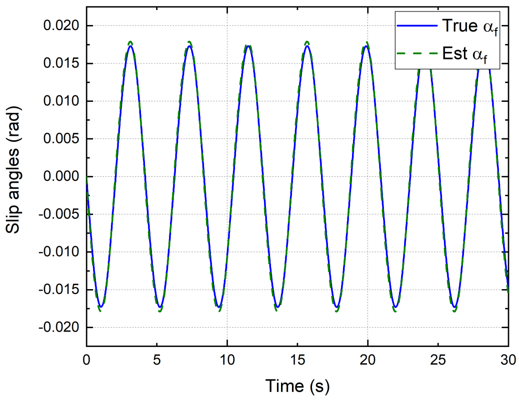

(c) Slip angle of front axle (Aligned)

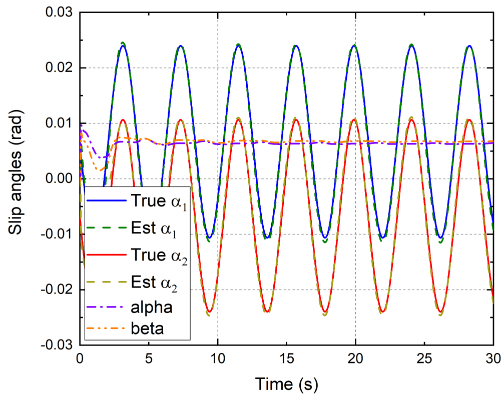

(d) Slip angle of each tire & offset (Aligned)

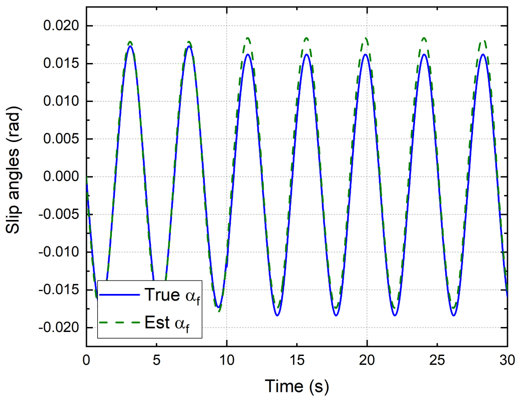

(e) Slip angle of front axle (Misaligned)

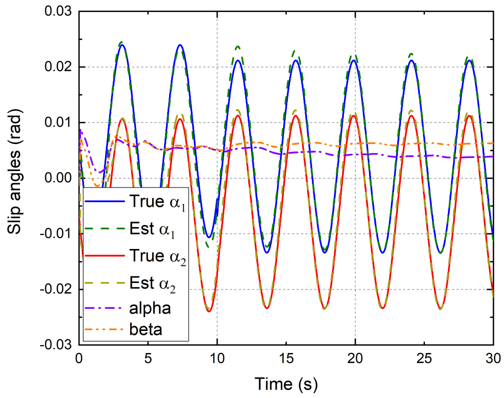

(f) Slip angle of each tire & offset (Misaligned)

Figure 8. Simulation results for detection of toe angle misalignment.

these conditions, detection is made for two scenarios. One scenario is a situation in which the toe angles of the two front axles are symmetrical. Another scenario is a situation in which the toe angle of the left wheel is suddenly changed due to a defect, and the toe angles of the left and right wheels are not symmetrical. The detection of toe angle misalignment should be made in this situation. The basic toe angle is set to the recommended values of 0.4 degrees on the left and right, respectively, based on the previous study (Guibin *et al.*, 2016). When a defect happens in the left wheel at 10 seconds, an error of -0.2 degree occurs. Accordingly, the left and right toe angle become to have a value of 0.2 and 0.4 degrees respectively. Here, a positive value means an angle in the direction of toe-in, and a negative value means an angle in the direction of toe-out. Figure 1 can be referred.

First, in a normal situation where the toe angles of the two front tires are symmetrical, Figure. 8(c) shows the slip angle of the front axle estimated through Equation (3) and the true slip angle. The estimated value is similar to the actual value with high accuracy. Based on this information, the slip angles of the left and right wheels that reflect the effect of the toe angle have been estimated. The results are shown in Figure 8(d). In addition, the $alpha$ and $beta$ offsets of each wheel slip angle regarding α_f are also shown in Figure 8(d). The estimated slip angles are very similar to the true slip angle of the left and right wheels, which includes both dynamics and the effect of toe angle. In addition, the values of $alpha$ and $beta$ converge to 6.77×10^{-3} rad, respectively, and it is almost identical to the toe angle set as a default value of 7.00×10^{-3} rad (0.4 degrees). That is, it can be concluded that the alignment of the toe angles is well done considering the each offset of the slip angle approximates the default value of the toe angle and is symmetrical with each other.

The second scenario is a situation in which the toe angle of the left wheel is misaligned from 0.4 to 0.2 due to a sudden defect at 10 seconds. Since the misalignment of the left wheel toe angle directly affects the value of α_f, it can be observed that the estimated α_f shows a large error from the actual α_f after 10 seconds as shown in Figure 8(e). Since Equation (3) cannot reflect the difference between each wheel, this error value cannot be corrected using α_f alone. Instead, it can be utilized as a reference point to obtain $alpha$ and $beta$ in the algorithm of this study. Figure 8(f) shows the estimated slip angle of the left and right wheels utilizing the value of α_f that is obtained from Equation (3). In addition, it also shows the each offset towards α_f which is $alpha$ and $beta$. Although the estimated α_f has an error with the true value after 10 seconds, the estimated slip angles of the left and right wheels reflecting the effect of the toe angle are almost identical to the actual values over time. One thing to notice is that $alpha$ and $beta$ converge to different values after 10 seconds. It confirms that the slip angles of the left and right wheels are no longer symmetrical. Furthermore, it can be observed that $alpha$ converges to a value smaller than $beta$. It proves not only that the toe angles of the left and right wheels are asymmetrical but the toe angles of the left wheel have become smaller than the original value after 10 seconds.

7. CONCLUSION

In this paper, an online toe angle misalignment detection system utilizing lateral tire force and tire aligning moment has been developed and evaluated through CarSim/Simulink co-simulation platform. The proposed system highlights the following unique points from the previously reported methods:

(1) By using the lateral tire force and tire aligning moment together, it is possible to analyze the effect of the toe angle acting on each wheel without complex suspension dynamics.
(2) Implementation of this system is realizable by only using readily available sensor signals on commercial vehicles.
(3) Unlike the pre-existing method of diagnosing wheel alignment, it focuses on real-time detection of the toe angle misalignment.

The simulation results prove that the proposed system can easily detect the toe angle misalignment while driving without any additional sensors or special tools.

ACKNOWLEDGEMENT−This research was partly supported by the BK21 FOUR Program of the National Research Foundation Korea (NRF) grant funded by the Ministry of Education (MOE); the National Research Foundation of Korea (NRF) grant funded by the Korea government (MSIP) (No. 2020R1A2B5B01001531); the Technology Innovation Program (20014983, Development of autonomous chassis platform for a modular vehicle) funded By the Ministry of Trade, Industry & Energy (MOTIE, Korea).

REFERENCES

Balike, K.P., Rakheja, S. and Stiharu, I. (2011). Development of kineto-dynamic quarter-car model for synthesis of a double wishbone suspension. *Vehicle System Dynamics* **49**, **1-2**, 107-128.

Cho, W., Yoon, J., Yim, S., Koo, B. and Yi, K. (2009). Estimation of tire forces for application to vehicle stability control. *IEEE Trans. Vehicular Technology* **59**, **2**, 638-649.

Choi, M. and Choi, S.B. (2014). Model predictive control for vehicle yaw stability with practical concerns. *IEEE Trans. Vehicular Technology* **63**, **8**, 3539-3548.

Choi, M., Oh, J.J. and Choi, S.B. (2013). Linearized recursive least squares methods for real-time identification of tire–road friction coefficient. *IEEE Trans. Vehicular Technology* **62**, **7**, 2906-2918.

Dechao, W. and Yaqing, T. (2007). An approach to measuring vehicle four-wheel alignment parameters based on computer vision. *Proc. IEEE 8th Int. Conf. on Electronic Measurement and Instruments,* 3-91.

D'Mello, G., Gomes, R., Mascarenhas, R., Ballal, S., Kamath, V.S. and Lobo, V.J. (2022). Wheel alignment detection with IoT embedded system. *Materials Today: Proceedings* **52**, 1924-1929.

Doumiati, M., Victorino, A., Charara, A. and Lechner, D. (2009). Virtual sensors, application to vehicle tire-road normal forces for road safety. *Proc. IEEE American Control Conf*, 3337-3343.

Erdogan, G., Alexander, L. and Rajamani, R. (2010). Estimation of tire-road friction coefficient using a novel wireless piezoelectric tire sensor. *IEEE Sensors Journal* **11**, **2**, 267-279.

Furferi, R., Governi, L., Volpe, Y. and Carfagni, M. (2013). Design and assessment of a machine vision system for automatic vehicle wheel alignment. *Int. J. Advanced Robotic Systems* **10**, **5**, 242-252.

Gadola, M., Chindamo, D., Romano, M. and Padula, F. (2014). Development and validation of a Kalman filter-based model for vehicle slip angle estimation. *Vehicle System Dynamics* **52**, **1**, 68-84.

Gajek, A. and Strzępek, P. (2016). The analysis of the accuracy of the wheel alignment inspection method on the side-slip plate stand. *In IOP Conference Series: Materials Science and Engineering* **148**, **1**, 012037.

Guibin, S.U.N., Youming, T.A.N.G., Yanmin, L.I. and Qian, P.E.N.G., 2016. Hard Points Optimization Design of Air Spring Suspension Based on Sensitivity Analysis. *Int. J. Simulation--Systems, Science & Technology* **17**, **43**, 20.1-20.8

Hahn, J.O., Rajamani, R. and Alexander, L. (2002). GPS-based real-time identification of tire-road friction coefficient. *IEEE Trans. Control Systems Technology* **10**, **3**, 331-343.

Henning, K.U. and Sawodny, O. (2016). Vehicle dynamics modelling and validation for online applications and controller synthesis. *Mechatronics* **39**, 113-126.

Hsu, Y.H.J., Laws, S.M. and Gerdes, J.C. (2009). Estimation of tire slip angle and friction limits using steering torque. *IEEE Trans. Control Systems Technology* **18**, **4**, 896-907.

Lee, E., Jung, H. and Choi, S. (2018). Tire lateral force estimation using Kalman filter. *Int. J. Automotive Technology* **19**, **4**, 669-676.

Lee, H. and Choi, S. (2022). Development of collision avoidance system in slippery road conditions. *IEEE Trans. Intelligent Transportation Systems.*

Ma, B., Lv, C., Liu, Y., Zheng, M., Yang, Y. and Ji, X. (2018). Estimation of road adhesion coefficient based on tire aligning torque distribution. *J. Dynamic Systems, Measurement, and Control* **140**, **5**, 051010.

Mananathan, R. (2021). *Automobile Wheel Alignment and Wheel Balancing*. 1st edn. SAE International. Warrendale.

Pacejka, H. (2005). *Tire and Vehicle Dynamics*. 2nd edn. Elsevier. Burlington.

Patel, H.H. (2016). *A study of parameters influencing the vehicle wheel alignment measurements.* Ph.D. dissertation. The University of North Carolina at Charlotte. Charlotte, North Carolina.

Rezaeian, A., Zarringhalam, R., Fallah, S., Melek, W., Khajepour, A., Chen, S.K., Moshchuck, N. and Litkouhi, B. (2014). Novel tire force estimation strategy for real-time implementation on vehicle applications. *IEEE Trans. Vehicular Technology* **64**, **6**, 2231-2241.

Spike, N., Bos, J., Beard, J. and Robinette, D. (2019). Wheel alignment effects on autonomous vehicle control vs human driver in simulation. *In Autonomous Systems: Sensors, Processing, and Security for Vehicles and Infrastructure* **11009**, 54-61.

Sulaiman, M.H., Sulaiman, S. and Saparon, A. (2021). IoT for wheel alignment monitoring system. *Int. J. Electrical & Computer Engineering* **11**, **5**, 3809-3817.

Teunissen, P. (2001). Dynamic Data Processing; Recursive Least Squares. 1st edn. Delft. DUP Blue Print.

Xu, N., Askari, H., Huang, Y., Zhou, J. and Khajepour, A. (2022). Tire force estimation in intelligent tires using machine learning. *IEEE Trans. Intelligent Transportation Systems* **23**, **4**, 3565-3574

Yasui, Y., Tanaka, W., Muragishi, Y., Ono, E., Momiyama, M., Katoh, H., Aizawa, H. and Imoto, Y., 2004. Estimation of lateral grip margin based on self-aligning torque for vehicle dynamics enhancement. *SAE transactions* **113**, **6**, 632-637.